A novel method to determine the FOCAL energy range

Dongqing Zhang (张冬青)[1,2], Xiangzhao Wang (王向朝)[1], and Weijie Shi (施伟杰)[1]

[1] *Information Optics Laboratory, Shanghai Institute of Optics and Fine Mechanics, Chinese Academy of Sciences, Shanghai 201800*

[2] *Graduate School of the Chinese Academy of Sciences, Beijing 100039*

Received March 17, 2005

Determination of the energy range is an important precondition of focus calibration using alignment procedure (FOCAL) test. A new method to determine the energy range of FOCAL off-lined is presented in this paper. Independent of the lithographic tool, the method is time-saving and effective. The influences of some process factors, e.g. resist thickness, post exposure bake (PEB) temperature, PEB time and development time, on the energy range of FOCAL are analyzed.

OCIS codes: 050.0050, 100.2550, 120.0120, 230.0230.

As the critical dimensions in the semiconductor industry are shrinking, fast and accurate *in-situ* measurements of projection optics aberrations of lithographic tools become increasingly necessary. Focus calibration using alignment procedure (FOCAL)[1−4] is an important technique used for self-calibration[5−8] of deep-ultraviolet (DUV) lithographic tools[9,10]. With this technique, imaging quality parameters, such as best focus, image tilt, field curvature, and so on, can be measured accurately. To acquire the parameters, the optimal exposure dose[11] which is chosen to expose the FOCAL marks onto the wafers should be available. To acquire the optimal exposure dose, FOCAL energy range must be obtained at first. Thus, determination of the energy range is one of the important preconditions of FOCAL test.

In the process of the periodic maintenance of lithographic tools, the FOCAL energy range is obtained by doing FOCAL procedure several times, which is time-consuming. Furthermore, when the test conditions such as illumination and process factors have some changes, the energy range will be altered and should be determined again. Hence, a more effective way to determine the energy range of FOCAL is needed.

In this paper, a new method to determine the FOCAL energy range is proposed. For FOCAL technique, FOCAL marks[12] on the FOCAL reticle should be exposed onto the wafer with the optimal exposure dose. In contrast to the symmetrical patterns of standard alignment mark[13], the FOCAL mark has asymmetrically chopped structures as shown in Fig. 1. After development of the exposed wafer, FOCAL mark positions are measured by alignment system[14]. For the existence of chop lines, intensity profile of aerial image of FOCAL mark changes as a function of defocus. This will induce different shifts to the measured alignment position when FOCAL mark is imaged with different focus offsets. The difference between the expected and the measured alignment position is alignment offset (AO) which also varies with defocus. The defocus with the maximum AO represents the best image offset. From the measured AO of FOCAL mark, best image offset can be calculated. By measuring the best image offset at about 90 different points of the image field, other imaging quality parameters (e.g. field curvature, image tilt, astigmatism, etc.) can be calculated accurately.

To determine the energy range of FOCAL, we discuss the relationship between the chop line width and defocus and analyze the requirement that the energy range needs to meet based on the experimental results and FOCAL theory as follows.

For FOCAL technique, the best image offset is determined from the measured AO values versus defocus. Therefore, the relationship between AO and defocus should be an important factor for us to determine the energy range of FOCAL.

An experiment of FOCAL test was performed on an ASML scanner with the optimal exposure dose. The experimental results were recorded and AO values under different defocus positions were obtained. The measured AO values under different defocus positions are shown in Fig. 2. The positive and minus signs mean the direction of defocus. The curve c was fitted from the measured AO.

From curve c, we know that AO decreases with the increase of defocus. The defocus corresponding to the maximum AO represents the best image offset. Thus, the best image offset at which all chops are printed properly can be found.

From Fig. 2, AO can be expressed as

$$\mathrm{AO} = a_0 + a_1\Delta f + a_2\Delta f^2 + a_3\Delta f^3 + \cdots + a_n\Delta f^n, \quad (1)$$

where Δf is the defocus of wafer, a_0, a_1, a_2, $\cdots$, a_n are the coefficients of the polynomial function.

The change of the printed chop line width causes variation of the intensity profile of alignment beam. This will bring a shift to the alignment position. Therefore, it is necessary to analyze the AOs under different chop line widths. We have

$$\mathrm{AO} = \frac{1}{2\pi f}\tan^{-1}\left(\frac{\exp(j2kd)\left(1-\cos(\omega a)+2\sum_{m=1}^{M}\sin(Br)\cdot\sin A\right)+2\sum_{m=1}^{M}\sin B\cdot\sin C+\cos(\omega c)-1}{\exp(j2kd)\left(\sin(\omega a)+2\sum_{m=1}^{M}\sin(Br)\cdot\cos A\right)+2\sum_{m=1}^{M}\sin B\cdot\cos C+\sin(\omega c)}\right), \quad (2)$$

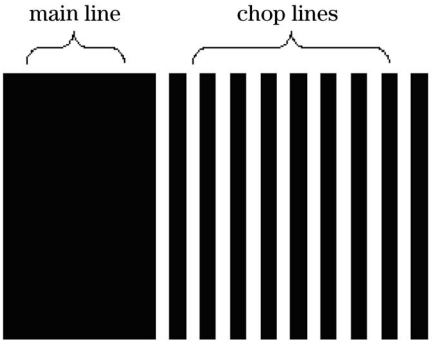

Fig. 1. Asymmetrically chopped structure of FOCAL mark.

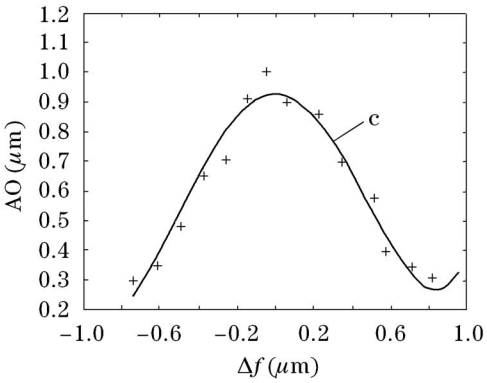

Fig. 2. Experimental results of AO.

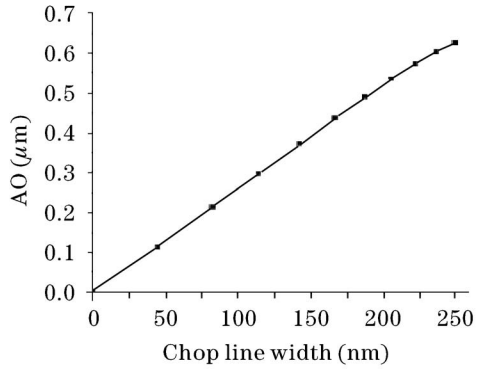

Fig. 3. AO versus the chop line width.

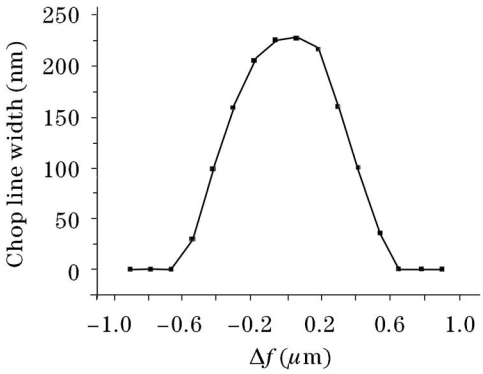

Fig. 4. Chop line width versus defocus.

where

$$A = 2\pi f\left(a + \frac{mL_{\mathrm{w}}}{M} - \frac{L_{\mathrm{w}}r}{2M(1+r)}\right),$$
$$B = \frac{\pi f L_{\mathrm{w}}}{M(1+r)},$$
$$C = 2\pi f\left(a + \frac{2m-1}{2M}L_{\mathrm{w}} - \frac{L_{\mathrm{w}}r}{2M(1+r)}\right),$$
$$k = \frac{2\pi}{\lambda}, \quad \omega = 2\pi\frac{1}{T}, \tag{3}$$

a, d are the line width and depth of the main line, respectively; c is the space width of the main grating; L_{w}, r, M are the line width, ratio of line to space, and number of the chop lines, respectively; T is the grating period; λ is the wavelength of alignment system.

Curve of the AO versus the chop line width can be obtained from Eqs. (2) and (3). As shown in Fig. 3, AO is proportional to the chop line width and can be expressed as

$$\mathrm{AO} = k \cdot L_{\mathrm{w}}, \tag{4}$$

where k is a proportion factor. From Eqs. (1), (2), and (4), the chop line width can be expressed as

$$L_{\mathrm{w}} = a'_0 + a'_1\Delta f + a'_2\Delta f^2 + a'_3\Delta f^3 + \cdots + a'_n\Delta f^n, \tag{5}$$

where Δf is the defocus of wafer, a'_0, a'_1, a'_2, $\cdots$, a'_n are the coefficients of the polynomial function, respectively. The curve of L_{w} versus defocus is shown in Fig. 4.

From the analysis above, the chop line width decreases with the increase of defocus for FOCAL technique. For the exposure doses within the FOCAL energy range, the corresponding curves of L_{w}-Δf have the characteristic that the chop line width is approximately at its maximum in the middle of the curve. This is the requirement that the exposure doses in the energy range need to meet. The positive resist optical lithography model PROLITH[15] can be used to simulate the curves of the chop line width versus defocus with different exposure doses. From the simulation results, the exposure doses which meet the requirement can be chosen. What's more, when determining the optimal exposure dose from the energy range of FOCAL, at least five measured points are expected on the AO-Δf curves. Because AO is proportional to the chop line width, there are at least five measured points on L_{w}-Δf curve. Therefore, if the focus offset and focus increment used in PROLITH are equal to that of FOCAL test, the simulated L_{w}-Δf curves which meet the above requirement and have at least five nonzero points are chosen. The corresponding exposure doses are within the energy range. By this method, the energy range of FOCAL can be determined. The dimension and the average dose of the energy range are expressed as Er and $\overline{\mathrm{Ed}}$

$$\begin{cases} \mathrm{Er} = E2 - E1 \\ \overline{\mathrm{Ed}} = \frac{E2+E1}{2} \end{cases}, \tag{6}$$

where $E1$ and $E2$ are the lower and upper limits of the range, respectively.

Curves of L_{w}-Δf with different exposure doses were simulated by PROLITH with numerical aperture NA =

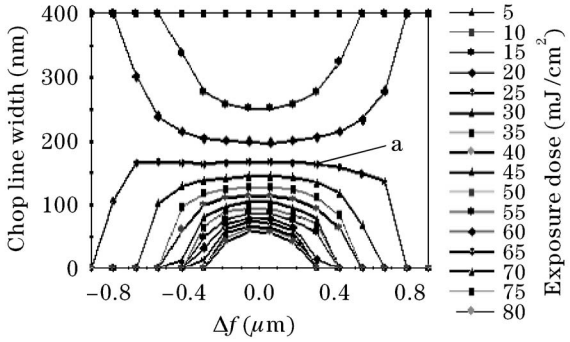

Fig. 5. Chop line width versus defocus with different exposure doses.

0.57, $\sigma = 0.75$, post exposure bake (PEB) temperature = 115 °C, PEB time = 60 s. Sixteen L_w-Δf curves were simulated with sixteen exposure doses. For different exposure doses, the chop line width changes in different ways with the increase of Δf, as shown in Fig. 5. For low exposure dose, the chop line width increases with the increase of Δf. For high exposure dose, the chop line width decreases with the increase of Δf. And for certain exposure dose, the chop line width does not change or changes minimally when Δf changes, such as curve a in Fig. 5.

For Fig. 5, when the exposure dose is higher than 30 mJ/cm^2, the chop line width decreases with the increase of Δf. When the exposure dose is lower than 65 mJ/cm^2, there are at least 5 nonzero points. Therefore, the energy range is 30—65 mJ/cm^2. From Eq. (6), the dimension and the average dose of the energy range was calculated. Er was 35 mJ/cm^2 and $\overline{\text{Ed}}$ was 47.5 mJ/cm^2.

When the process conditions of FOCAL test change, the energy range needs to be determined again. The energy ranges for different process factors, e.g. resist thickness, PEB time, PEB temperature and development time, are analyzed as below.

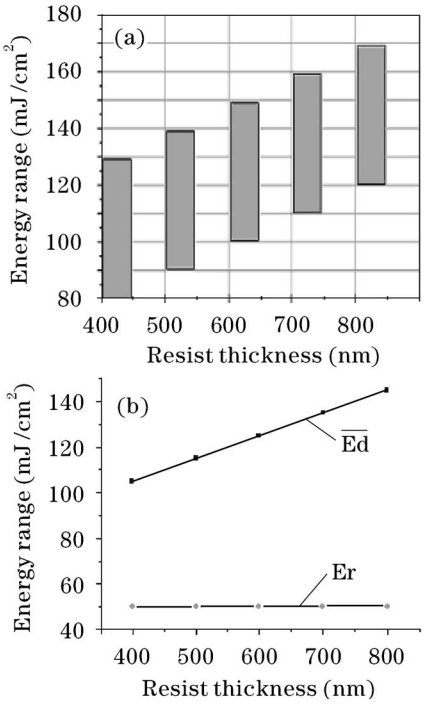

Fig. 6. Energy range versus the photoresist thickness.

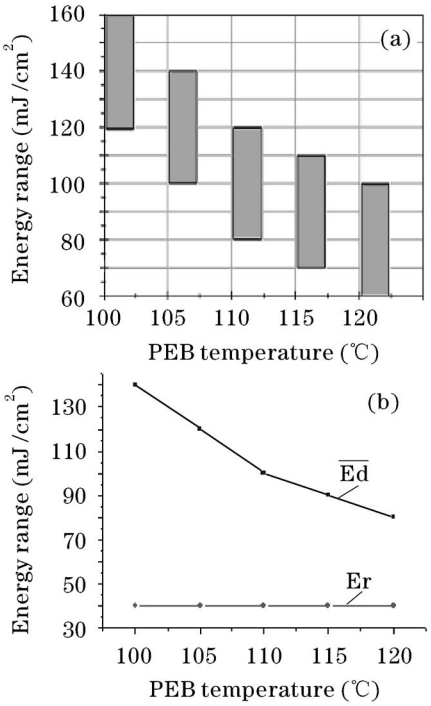

Fig. 7. Energy range versus the PEB temperature.

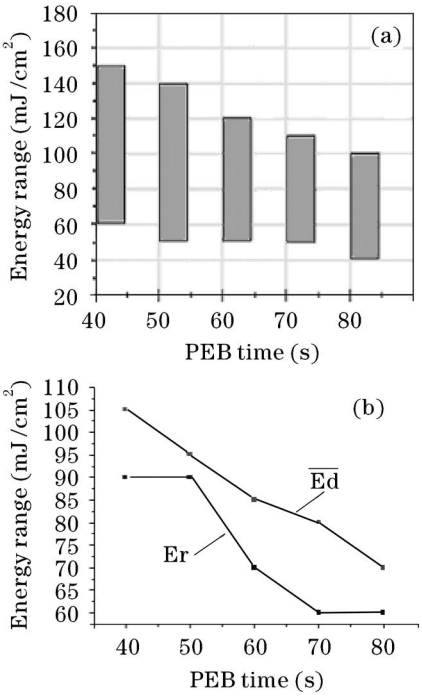

Fig. 8. Energy range versus the PEB time.

The L_w-Δf curves were simulated using PROLITH when the resist thickness was 400, 500, 600, 700, 800 nm, respectively. Using the method presented in the paper, the energy ranges for different resist thicknesses were determined. The energy ranges are shown as different rectangles in Fig. 6(a). For example, the energy range is 80—130 mJ/cm^2 as the resist thickness is 500 nm. The

energy range is 120—170 mJ/cm^2 as the resist thickness is 800 nm. From Fig. 6(b), we know that $\overline{\mathrm{Ed}}$ increases and Er does not change when the resist thickness increases.

The L_{w}-Δf curves were simulated when the PEB temperature was 100, 105, 110, 115, and 120 °C, respectively. The energy ranges are shown as different rectangles in Fig. 7(a). From Fig. 7(b), it can be seen that $\overline{\mathrm{Ed}}$ decreases and Er does not change when the PEB temperature increases. Similarly, the L_{w}-Δf curves were simulated when the PEB time was 40, 50, 60, 70, and 80 s, respectively. The energy ranges with different PEB times were shown in Fig. 8(a). From Fig. 8(b), it can be seen that $\overline{\mathrm{Ed}}$ and Er both decrease when the PEB time increases.

The L_{w}-Δf curves were simulated when the development time was 40, 50, 60, 70, and 80 s, respectively. The energy ranges with different development times were shown in Fig. 9. From this figure, it can be seen that FOCAL energy range does not change when the development time is longer than 50 s.

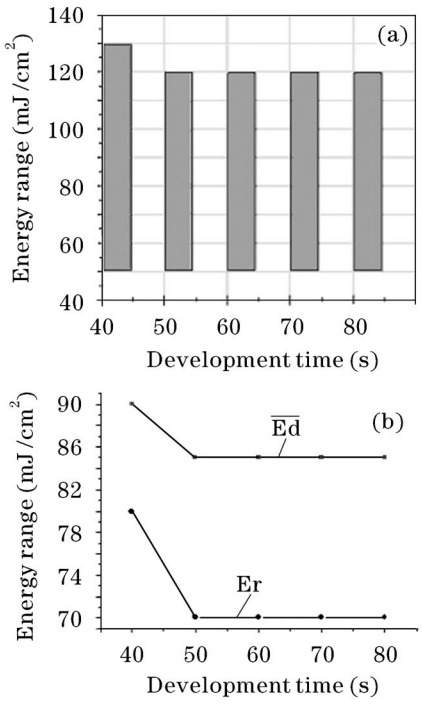

Fig. 9. Energy range versus the development time.

A new method to determine the FOCAL energy range has been presented based on the relationship between the FOCAL chop line width and defocus. Curves of the chop line width versus defocus were simulated by PROLITH. By choosing the curves which satisfy certain conditions, the energy range of FOCAL can be determined off line. The influences on the energy range of the resist thickness, PEB temperature, PEB time and development time have been analyzed in the paper. In contrast to PEB time, the resist thickness, PEB temperature and development time have less influence on the dimension of the FOCAL energy range. The average dose of the energy range decreases with the reduction of resist thickness and increases when the PEB temperature gets lower. The new method is reliable, simple, time-saving and independent of the lithographic equipment.

D. Zhang's e-mail address is zdq@siom.ac.cn.

References

1. E. L. Raab, C. Pierrat, and C. H. Fields, Proc. SPIE **2197,** 550 (1994).
2. T. E. Adams, Proc. SPIE **1464,** 294 (1991).
3. W. Shi, X. Wang, D. Zhang, F. Wans, and M. Ma, Proc. SPIE **5645,** 233 (2005).
4. B. Vleeming, B. Heskamp, H. Bakker, L. Verstappen, J. Finders, J. Stoeten, R. Börret, and O. Roempp, Proc. SPIE **4346,** 634 (2001).
5. D. G. Flagello and B. Geh, Proc. SPIE **2724,** 788 (1996).
6. T. Hagiwara, H. Mizutani, N. Kondo, J. Inoue, K. Kaneko, and S. Higashibata, Proc. SPIE **4346,** 1635 (2001).
7. F. Wang, X. Wang, M. Ma, D. Zhang, and W. Shi, Laser & Optoelectronics Progress (in Chinese) **41,** (6) 34 (2004).
8. N. R. Farrar, A. L. Smith, D. Busath, and D. Taitano, Proc. SPIE **4000,** 18 (2000).
9. H. E. Mayer and E. W. Loebach, Proc. SPIE **811,** 149 (1987).
10. X. Chen, H. Yao, and X. Chen, Chin. Opt. Lett. **2,** 187 (2004).
11. P. Dirksen, W. de Laat, and H. Megens, Proc. SPIE **2440,** 701 (1995).
12. P. Dirksen, R. Pellens, and C. Juffermans, Proc. SPIE **2726,** 799 (1996).
13. G. Bouwhuis and S. Wittekoek, IEEE Trans. Electron. Devices **26,** 723 (1979).
14. N. Ishio, K. Fujiwara, and H. Nagata, Proc. SPIE **1264,** 578 (1990).
15. C. A. Mack, Proc. SPIE **538,** 207 (1985).